Selective Aerobic Oxidation of Lactate to Pyruvate Catalyzed by Vanadium-Nitrogen-Doped Carbon Nanosheets

Zhang, W.; Oulego, P.; Slot, T.K.; Rothenberg, G.; Shiju, N.R.

DOI
10.1002/cctc.201900819

Publication date
2019

Document Version
Final published version

Published in
ChemCatChem

ChemPubSoc Europe

DOI: 10.1002/cctc.201900819

CHEMCATCHEM Communications

Selective Aerobic Oxidation of Lactate to Pyruvate Catalyzed by Vanadium-Nitrogen-Doped Carbon Nanosheets

Wei Zhang,[a] Paula Oulego,[b] Thierry K. Slot,[a] Gadi Rothenberg,[a] and N. Raveendran Shiju*[a]

The catalytic oxidative dehydrogenation of lactates with molecular oxygen is a promising yet challenging route for producing high-value pyruvates from biomass. Here we report a simple synthetic strategy for preparing nitrogen-doped carbon nanosheets (NCNs) starting from two abundant precursors, cheap melamine and glucose, and using a simple thermal-annealing process. The resulting NCNs feature numerous edges and holes for anchoring vanadium oxides (V-NCNs). This creates cooperative catalytic sites that boost the catalytic oxidation of ethyl lactate to ethyl pyruvate. Additionally, we systematically studied the surface nitrogen species of NCNs by varying the pyrolysis temperature, and found that the active pyridinic N-oxide species formed in a high thermal-annealing treatment, acting synergistically with vanadium active sites in converting ethyl lactate with oxygen into ethyl pyruvate under mild conditions.

Lignocellulosic biomass platform molecules are valid sustainable feedstocks for many value-added chemicals. They can replace fossil raw materials, because the volumes of biomass produced can match the demand for chemicals (this is not true for fuels).[1–2] A good example is lactic acid and lactates, which are already produced on a large scale from biomass fermentation.[3] Lactates can be converted into various commodity chemicals, including acrylic acid, pyruvic acid and pyruvates, lactide, acetaldehyde and propanediol.[4–5] In particular, pyruvate esters are important chemicals used in many sectors, including agrochemicals, foodstuffs, cosmetics, and pharmaceuticals.[6–7] Pyruvate is a key metabolite, and is biologically produced from sugars by microorganisms.[8–9] However, the main drawback of metabolic route is its low productivity and costly purification of pyruvate.[10]

[a] W. Zhang, T. K. Slot, Prof. Dr. G. Rothenberg, Dr. N. R. Shiju
Van't Hoff Institute for Molecular Sciences
University of Amsterdam
Science Park 904, 1098 XH Amsterdam (The Netherlands)
E-mail: n.r.shiju@uva.nl
Homepage: http://hims.uva.nl/hcsc
[b] Dr. P. Oulego
Department of Chemical and Environmental Engineering
University of Oviedo
C/ Julián Clavería, s/n. 33071, Oviedo (Spain)

Supporting information for this article is available on the WWW under https://doi.org/10.1002/cctc.201900819

Alternatively, pyruvates can be produced by direct oxidative dehydrogenation of lactates with molecular oxygen (eq 1). This route is more sustainable than the currently used pyrolysis of tartaric acid with stoichiometric $KHSO_4$ as a dehydrating agent.[11–12] But the direct aerobic oxidation of lactate to pyruvate is a challenging process. Oxygen is the most abundant and the cheapest oxidant, but its high activation barrier and its tendency to form free-radicals means that the pyruvate product is easily over-oxidized.[13] This over-oxidation can be suppressed, but that typically requires expensive noble-metal catalysts, such as Pd or Pt.[14–16] For practical purposes, as well as from a sustainability viewpoint, abundant-element catalysts are preferred. Several catalysts were reported, including iron phosphates,[17–19] single oxides (ZrO_2 and SnO_2)[17] and binary oxides (*e.g.*, Ni–Nb–O, SnO_2–MoO_3 and Fe_2O_3–MoO_3, and MoO_3–TiO_2)[18–21] as well as MoVNbO based complex oxides[22–23]

Vanadium is a suitable option, as its availability is high and its toxicity is low. Moreover, with a molecular weight of just 50.9, a low-loading vanadium catalyst has only a small ecological footprint. Mae *et al.* found that vanadium oxytrichloride ($VOCl_3$) can catalyze the aerobic oxidation of ethyl lactate to ethyl pyruvate at room temperature, but $VOCl_3$ is unstable and easily hydrolyzed by the water byproduct.[24] Vanadium-based catalysts are also easily recovered, simplifying product purification.[25]

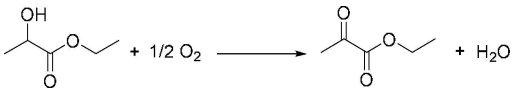

Addressing these problems, we studied a series of supported vanadium oxides in the conversion of lactates to pyruvates, and found that titania-supported vanadia outperformed other supports.[26] We also found that adding a small amount of activated carbon can inhibit the ethyl pyruvate polymerization in the titania-catalyzed oxidation of ethyl lactate.[27] Recently, we demonstrated that vanadia supported on activated carbon can act synergistically with homogeneous pyridine additives in the aerobic oxidation of ethyl lactate to ethyl pyruvate, giving high conversion and selectivity.[28] Based on these findings, we hypothesized that integrating the vanadia sites into nitrogen-doped carbon (NCs) structures could give efficient heterogeneous catalysts for the selective oxidation of lactate to pyruvate under mild conditions.

Nitrogen-doped carbons are readily prepared by pyrolysing various nitrogen-rich precursors together with carbon. The nitrogen dopant plays a vital role in the surface activation of

dioxygen, boosting the efficiency of the carbon-based catalyst.[29–30] Moreover, the electron-rich character of nitrogen-doped carbons facilitates the anchoring of metal/metal oxide active sites, thereby enhancing catalytic performance.[31] Inspired by this, we prepared nitrogen-doped carbon nanosheets (NCNs) using melamine and glucose as precursors via a simple two-step process. These NCNs are excellent supports for anchoring vanadium oxides. The resulting V-NCNs catalysts, combining abundant nitrogen dopants and well-dispersed vanadium sites, showed a synergistic effect, improving their catalytic activity in the selective aerobic oxidation of lactate to pyruvate. Moreover, owing to the strong interaction between vanadium and nitrogen dopant, the V-NCNs are stable and can be reused at least five times without losing any activity.

Scheme 1 outlines the synthesis of vanadia-nitrogen co-doped carbon nanosheets (V-NCNs). First, we prepared nitrogen-doped carbon nanosheets (NCNs) by a simply pyrolysing various nitrogen-rich precursors together with carbon. For this, we hydrothermally treated a mixture of melamine, glucose and Pluronic® F-127 at 180 °C for 12 h, followed by a pyrolysis process at 800 °C. Melamine is an abundant and non-toxic nitrogen precursor, which can form C_3N_4 fragments in the glucose-derived carbon matrix during the hydrothermal process. These fragments provide nitrogen atoms doped in the carbon skeleton, and decompose at 600–700 °C, yielding N-doped nanosheets.[32] Vanadium oxides were then supported onto the NCN supports by wet impregnation of an ethanolic solution of vanadyl acetylacetonate, $VO(acac)_2$, followed by drying and calcining (see the experimental section in the Supporting Information for details).

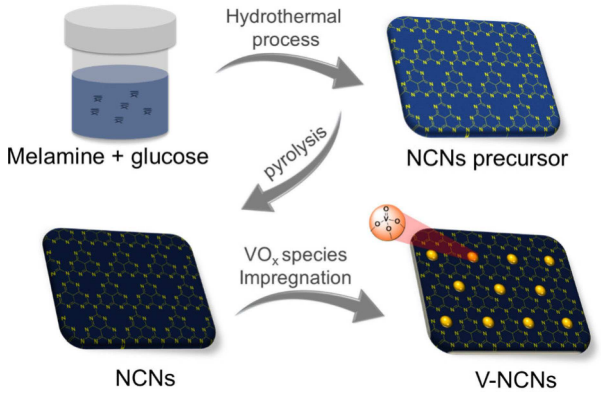

Scheme 1. The synthesis route to nitrogen-doped carbon nanosheet supports (NCNs) and their combination with vanadium oxide to give V-NCNs.

Transmission electron microscopy (TEM) of the NCNs shows ultrathin sheet-like morphology with many wrinkles in large domains (Figure 1a). High-resolution TEM shows numerous nanoholes in the sheet structure (Figure 1b). Adding Pluronic® F-127 as the soft template leads to the formation of mesopores. The polymerization of melamine precursor occurred during the hydrothermal synthesis, which was confirmed by Fourier-transform infrared spectroscopy (FTIR). As shown in Figure S1, the characteristic absorption band of *s*-heptazine units (~810 cm^{-1}) was detected for NCN precursor, confirming the *in-situ* formed polymeric carbon nitride.[33] Subsequent pyrolysis removed the C_3N_4 fragments, leading to the formation of nanoholes. This was verified by the disappearance of the heptazine vibration at a high pyrolysis temperature (up to 800 °C).

The average pore sizes of V-NCNs materials decrease as follows (see Table S1): V-NCN-900 (48 nm) ≈ NCN-800 (45 nm) > NCN-700 (14 nm) ≈ NCN-600 (13 nm). This agrees with the FTIR results and confirms that the enlarged pores are caused mainly by the decomposition of carbon nitride when the temperature was increased to 800 °C. The wrinkles of sheet-like structures consist of 8–9 nitrogen-doped carbon layers (Figure 1c). The NCNs sample was further loaded with vanadium and annealed in argon at 400 °C for 4 h, yielding vanadium-nitrogen co-doped carbon nanosheets (V-NCNs). The analysis of the morphology of V-NCNs-800 catalyst by the scanning transmission electron microscopy (STEM) indicates that the ultrathin nanosheet remains stable when vanadia was introduced in NCNs support (Figure 1d). The corresponding energy-dispersive X-ray spectroscopy (EDX) elemental mapping (Figure 1, e–h) showed that the elements V, N, C and O were homogeneously distributed over the V-NCNs-800 nanosheets. The selected area electron diffraction (SAED) image of V-NCNs-800 shows a set of diffraction rings of graphic carbon (Figure 1i), implying that amorphous vanadia species are well dispersed on the NCNs surface.

We then tested the V-NCNs catalysts in the oxidative dehydrogenation of ethyl lactate to ethyl pyruvate. Previously, we showed that adding molecular sieve3A (MS 3A) as a dehydrating agent can suppress the competing hydrolysis, giving a much higher selectivity to pyruvate.[25] In a typical reaction, ethyl lactate (5 mmol) and oxygen (1 atm) were reacted in the presence of 25 mg of V-NCNs catalyst (together with 1 ml diethyl succinate as the solvent and 100 mg MS 3A) at 130 °C for 9 h. Control experiments confirmed that the pristine NCNs (without vanadium) were inactive, giving only 5% conversion of the background thermal reaction. Loading the NCNs with ~1.0 wt.% vanadium (determined by ICP analysis) increased the conversion to 99%! (Figure 2). This shows that these novel integrated V-NCNs catalysts combining abundant nitrogen dopant and well-dispersed vanadium sites showed high efficiency as synergistic catalysts for selective aerobic oxidation of lactate to pyruvate. More importantly, owing to the strong interaction between vanadium and nitrogen dopant, the V-NCNs catalysts are stable and can be reused at least five times without losing any activity, showing superior durability and recyclability.

To validate the nitrogen surface effect, we prepared pure carbon nanosheets via the same method yet without the nitrogen precursor (denoted as CNs, see Figure S2). The nitrogen-free CNs supported vanadia (V-CNs) gave only 60% conversion under otherwise identical conditions. This shows that the surface nitrogen species play a vital role in the catalytic oxidation of ethyl lactate. To prove this, we prepared separate samples of vanadium oxide supported on mesoporous graphitic carbon nitride (V-mpg-C_3N_4). The surface vanadium content of these samples was identical to that of the V-NCNs (detailed

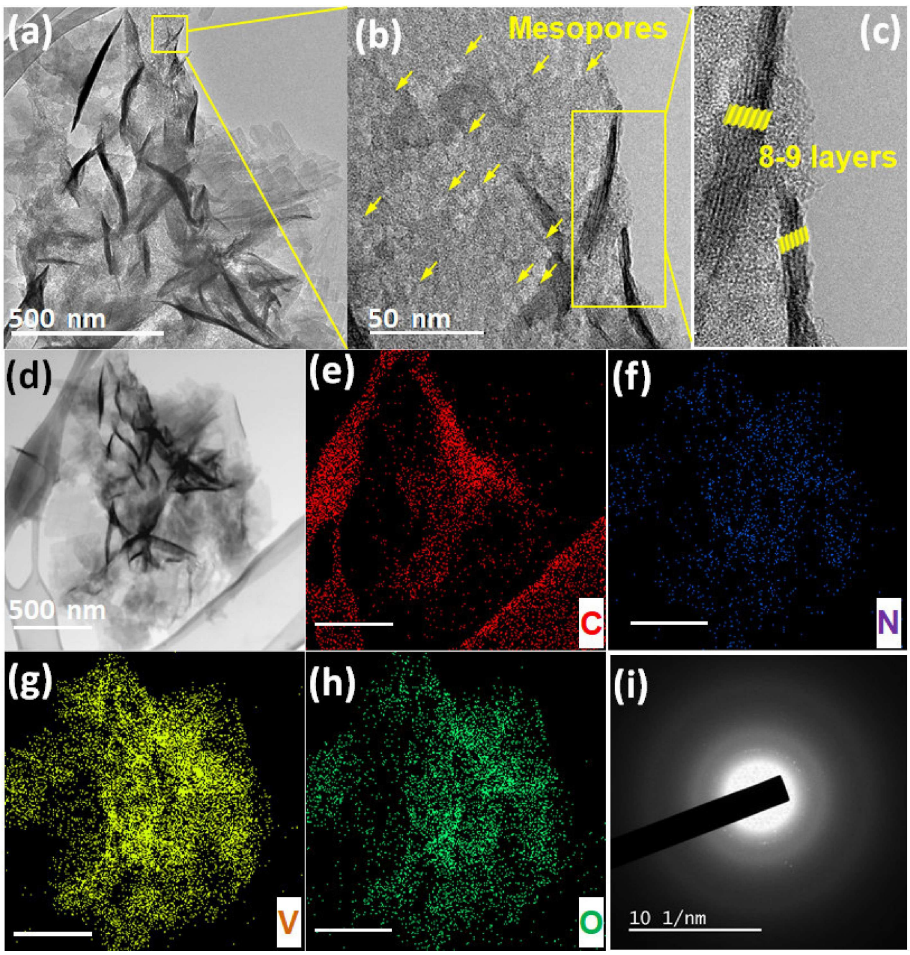

Figure 1. (a) TEM image of nitrogen-doped carbon nanosheets (NCNs-800) (b) representative high-resolution TEM images of NCNs-800, with yellow arrows marking mesopores (c) magnified HRTEM image showing the lamellar stacking of the nanosheets (d) STEM image of NCNs-800 supported vanadia catalyst (V-NCNs-800) (e–h) the corresponding element mapping of V, C, N and O in V-NCNs-800 catalyst (i) SAED image of V-NCNs-800 (note: V-NCNs-800, pyrolysis at 800 °C).

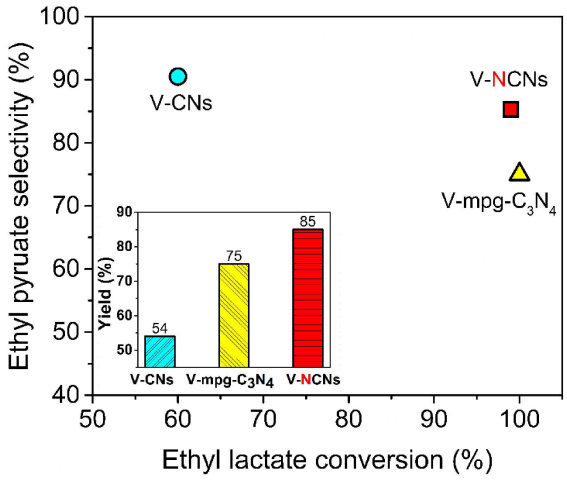

Figure 2. Selectivity to ethyl pyruvate plotted against ethyl lactate conversion over three supported vanadium oxide catalysts: V-CNs (cyan), V-mpg-C_3N_4 (yellow) and V-NCNs (red). The inset shows the corresponding ethyl pyruvate yield. Reaction conditions: ethyl lactate 5 mmol, catalyst 25 mg, 1 atm O_2, diethyl succinate (solvent, 1 ml), molecular sieve-3 Å (dehydrating agent, 100 mg), 130 °C, 9 h.

experimental procedures are included in the Supporting Information). As shown in Figure 2, V-mpg-C_3N_4 gave a quantitative conversion of ethyl lactate but with more side-products, affording only 75% of ethyl pyruvate compared to the 85% obtained with V-NCNs. Note that vanadia supported on pure carbon nanosheets showed the highest *selectivity* to ethyl pyruvate of 91%, confirming our earlier observations that the presence of carbon favors the production of ethyl pyruvate.[27–28] We therefore conclude that combining vanadia active sites with nitrogen-rich carbon support creates cooperative catalysts,[34] boosting the catalytic oxidation of ethyl lactate to ethyl pyruvate.

The pyrolysis temperature can impact the nitrogen species in NCNs supports, affecting the catalytic activity.[35] We studied this influence by varying the pyrolysis temperature of the NCNs. The resulting supports are denoted as NCNs-x, where x represents the pyrolysis temperature (600–900 °C). Using these supports, we prepared the corresponding vanadium oxide catalysts (V-NCNs-x) under identical conditions. All four V-NCNs-x samples were highly active, giving ethyl pyruvate with high

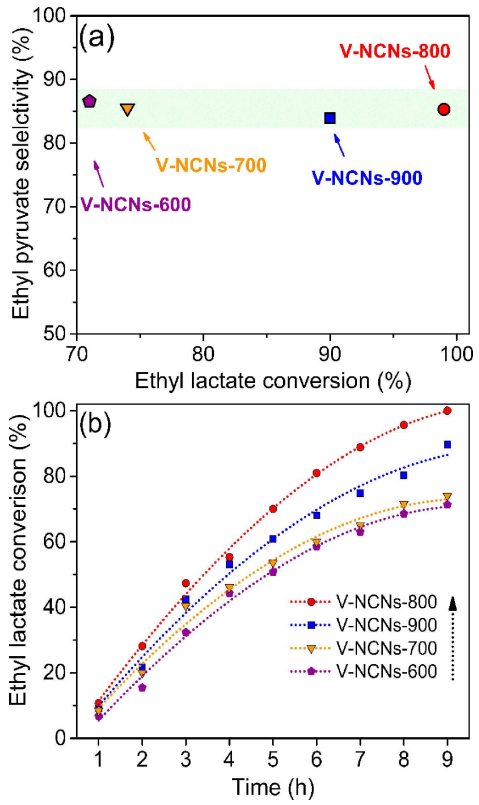

Figure 3. (a) Comparisons of the aerobic oxidation of ethyl lactate to ethyl pyruvate over the various V-NCNs-x catalyst. Reaction conditions: ethyl lactate 5 mmol, catalyst 25 mg, 1 atm O_2, diethyl succinate (solvent, 1 ml), molecular sieve-3 Å (dehydrating agent, 100 mg),130 °C and 9 h. (b) The time-resolved conversion profile of ethyl lactate over the V-NCNs-x catalysts.

selectivity (Figure 3a). The activity order was V-NCNs-800 > V-NCNs-900 > V-NCN-700 > V-NCN-600, showing the importance of the pyrolysis temperatures. Plotting the reaction profiles for these catalysts confirmed the trend (Figure 3b), showing that a pyrolysis temperature of 800 °C was optimal for converting lactate to pyruvate.

To understand this effect further, we ran ex-situ X-ray photoelectron spectroscopy (XPS) measurements to probe the surface chemical composition and valence states in NCNs-x samples varying at different pyrolysis temperatures ranging from 600–900 °C. As shown in Figure 4a, the N 1s signals of NCNs-x samples can be fitted with several peaks, reflecting the existence of six different nitrogen forms in the materials (Figure 4, b-c): pyridinic-N or sp^2-hybridized-N in triazine rings (N1, ~398.7 eV, red), pyrrolic-N (N2, ~399.8 eV, green), amino-N (N3, ~400.6 eV, yellow), quaternary-N or graphitic-N (N4, ~401.3 eV, pink) and pyridine oxide-N (N5, ~403.5 eV, blue), respectively.[36–38]

We found that the pyrolysis temperatures affect the nitrogen species in NCNs surface. For the NCNs-600, two deconvoluted peaks belong to sp^2 hybridized N and bridging amino N in tri-s-triazine periodic networks (N1 and N3), respectively.[39–40] As the pyrolysis temperature increased, the triazine structure started to decompose and converted into other nitrogen species. The characteristic peaks of amino groups (N3) disappeared at 700 °C, accompanying two new N signals of pyrrolic-N (N2) and graphitic-N (N4). When the temperature increased to 800 °C, nitrogen dopant was gradually converted to pyridine-N oxide (N5). The thermal transformation was also reflected by C1s spectra (Figure 4d). The spectrum of C1s in NCNs-600 can be deconvoluted into two components including adventitious C (~284.6 eV), C–N (~286.6 eV) and sp^2-bonded C (N=C–N, ~287.8 eV). Further increased the pyrolysis temperature, new peaks located at 289.1 eV and 291.16 eV can be attributed to C–O and C=O species, respectively. Again, note that the XPS data is not *in-situ*, therefore the correlation can serve only for orientative purposes.

We ran Raman spectroscopy to detect the degree of graphitization in V-NCNs-x samples. As shown in Figure 4e, all the samples showed two bands centered at 1338 and 1592 cm^{-1}, assigned to the disordered/defected carbon (D band) and graphitic sp^2 carbon (G band), respectively.[41–42] For V-NCNs-600, the peak intensity ratio of I_D/I_G was determined to be 0.81 suggesting a graphitic structure, in agreement with the XRD results (Figure S3).[32] By comparison, the I_D/I_G was remarkably increased to 0.95, 0.95 and 0.97 for V-NCNs-700, V-NCN-800 and V-NCNs-900, respectively, indicating an increase in the defect and disorder degree with pyrolysis temperature.[43] Finally, we examined the bulk structure using powder X-ray diffraction (PXRD, Figure S3). In all four cases, no crystalline vanadia peaks are detected, which is in good agreement with the SAED pattern (Figure 1i).

Based on the above results, we reasoned that higher pyrolysis temperatures (800–900 °C) lead to an increase in the graphitization degree, forming nitrogen-doped carbon nanosheets with abundant edges and holes. However, various nitrogen types were formed in NCs including pyridinic N, pyrrolic N, quaternary N and pyridine-N-oxide, and the role of each nitrogen remains unclear.[44] Previously, Wang[45] and Cao[46] reported that the *pyridinic* nitrogen was responsible for the enhanced efficiency of Pd/NCs catalysts. Beller *et al.* identified the *graphitic* nitrogen as the active promoter in the hydrogenation of arenes over Ru/CNs catalysts.[47] In our case, there is no clear correlation between the catalytic activity and the amount of pyridinic or graphitic nitrogen. Notably, we found that more nitrogen species in NCNs were oxidized to pyridinic-N–O starting from 800 °C (see Figure 4). We hypothesize that the new oxidized N active sites could stabilize the vanadium sites and tune their electronic properties, thereby favoring the catalytic efficiency.[48]

To check this hypothesis, we studied the catalytic performance of V-NCNs-x catalysts by comparing the turnover frequency (TOF) at low conversions (< 15%). As shown in Figure 5a, the TOFs of the oxidation reaction on V-NCNs-x catalysts are proportional to the pyrolysis temperature of the NCN supports. Moreover, despite the higher nitrogen content and specific surface area in V-NCNs-600 and V-NCN-700, their TOFs are lower compared to V-NCNs-800 and V-NCN-900. We also plotted the area-specific conversion rate of ethyl lactate (r_{EL}, the right axis in Figure 5a) against the pyrolysis temperature. Clearly, with a temperature of below 700 °C, the r_{EL} almost

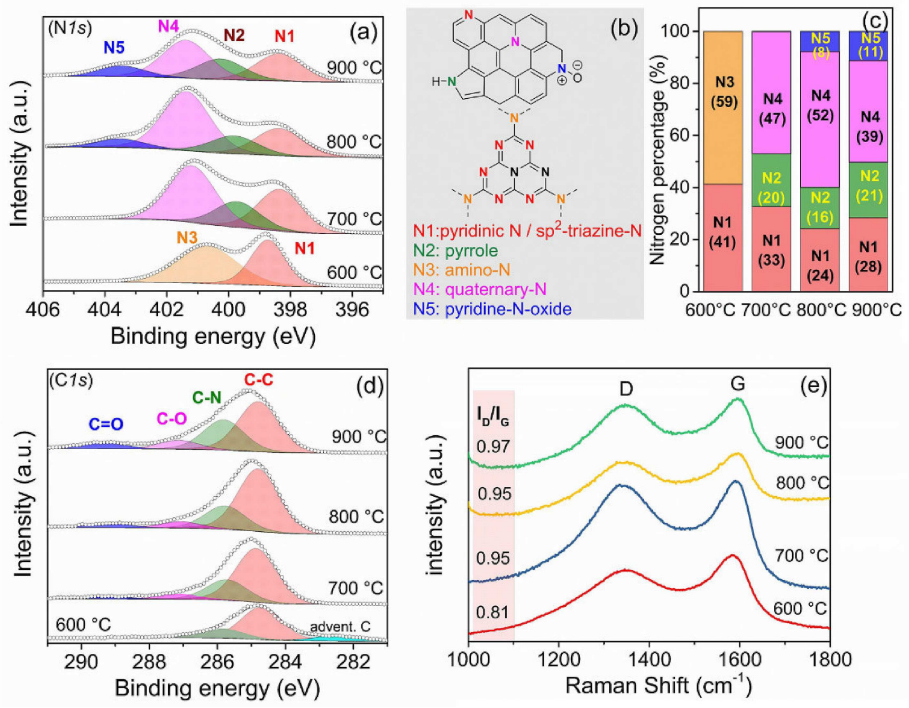

Figure 4. (a) XPS spectra of N 1s in the V-NCNs-x catalysts (x = 600, 700, 800 and 900 °C) (b) types of nitrogen functionalities occurring in V-NCNs-x samples and (c) nitrogen contents of NCNs-x with different pyrolysis temperatures (N1: sp^2 hybridized-N, red; N2: pyrrolic-N, green; N3: amino-N, yellow; N4: graphitic-N, pink; N5: pyridine oxide-N, blue). The nitrogen species were quantified based on XPS data of the materials treated at different temperatures. (d) high-resolution C 1s spectra of V-NCNs-x. (e) Raman spectra of V-NCNs-x samples.

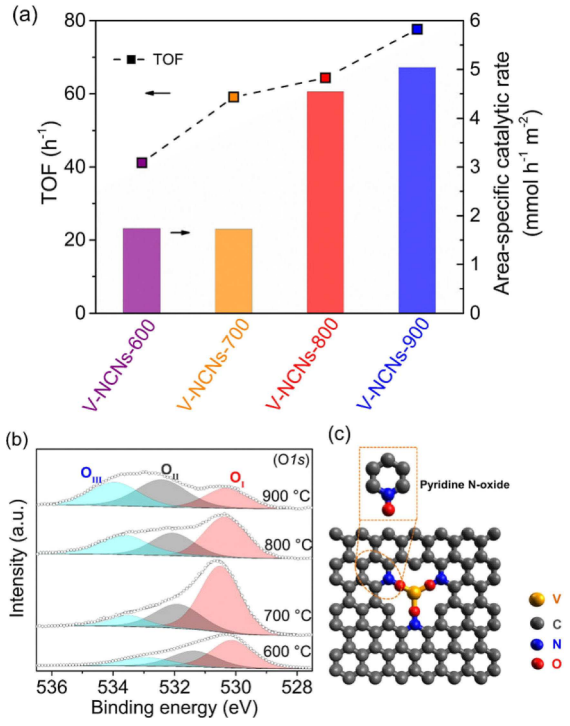

Figure 5. (a) Comparison of TOF of ethyl lactate oxidation and area-specific conversion rate of ethyl lactate over the V-NCNs-x catalysts. (b) High-resolution O 1s spectra of V-NCNs-x samples. (c) Schematic diagram of pyridine N-oxide in the V-NCNs-900 catalyst.

leveled up. Increasing the temperature to 800 °C gave r_{EL} of 4.5 mmol $h^{-1}m^{-2}$, which is thrice than that of V-NCNs-700 (r_{EL} = 1.72 mmol $h^{-1}m^{-2}$). Annealing at 900 °C (V-NCNs-900) increased the area-specific conversion rate of ethyl lactate to 5.0 mmol $h^{-1}m^{-2}$. This may reflect the oxidized-N content increase from 8% to 11% (see Figure 4c).

As shown in Figure 5b, the spectra of O 1s in V-NCNs-x can be fitted into three peaks: the peaks at 530.5 eV and 531.7 eV represent the vanadia lattice oxygen (O_I) and the chemisorbed oxygen(O_{II}), respectively;[26] The peak at 533.7 eV was attributed to the pyridinic N-oxygen or carbonyl oxygen (O_{III}), in which the pyridinic N-oxide species dominate at high temperature (> 800 °C).[48–50] In our case, the atom ratio of $O_{III}/(O_I + O_{II} + O_{III})$ in these series increased as follows: V-NCNs-900 (0.33) > V-NCNs-800 (0.30) > V-NCNs-700 (0.19) > V-NCNs-600 (0.11), in good agreement with the catalytic efficiency in Figure 5a. This indicates that the oxidized N plays a key role. Furthermore, the surface variation of nitrogen dopant also affects the electron charge density of vanadium sites. The V $2p_{3/2}$ peak can be deconvoluted into three distinct peaks at 516.2 eV, 517.3 eV and 518.2 eV, corresponding to V^{3+}, V^{4+} and V^{5+} species, respectively (Figure S4). The $V^{5+}/(V^{3+} + V^{4+} + V^{5+})$ ratio gradually decrease from 0.41 to 0.23 when the temperature is increased from 600 to 900 °C, implying more surface V species are reduced by the nitrogen dopant. The increased redox V active sites are beneficial for the catalytic oxidation reaction.[25] We conclude that the catalytic performance is determined by the structure of surface nitrogen species, and particularly by the

pyridinic N-oxide species located at the defects are more active for the oxidation, acting synergistically with vanadium active sites (Figure 5c).

Recycling experiments were run for the V-NCNs-800 catalysts. In each cycle, the catalyst was filtered, washed with acetone and deionized water, and dried at 100 °C. Figure S5 showed that V-NCNs-800 can be reused at least five times without significant loss of activity, keeping ethyl lactate conversion at >90%. We also characterized the V-NCNs-800 catalyst after reusing five times. The TEM analysis shows that the nanosheet structure of reused sample was preserved (Figure S6). Additionally, the Raman spectra of the fresh and the fifth-used catalyst are identical (Figure S7). The nitrogen-free V-CNs sample shows a set of bands typical of crystalline vanadium oxide,[51] while the V-NCNs-800 only gave a weak band at ~1050 cm^{-1} characteristic of isolated V=O species.[52] This indicates that nitrogen doping facilitates the formation of isolated vanadia. Only a slight decrease in ethyl lactate conversion was observed at the fifth run, which agrees well with the marginal decrease in vanadium loading (from 1.2 wt.% to 1.0 wt.%, measured by ICP-AES analysis, see Table S1).

In summary, we have prepared nitrogen-doped carbon nanosheets (NCNs) from melamine and glucose precursors via a simple thermal-annealing process. These supports have multiple edge and vacancy sites and are excellent for anchoring vanadium oxides, boosting the catalytic efficiency for the aerobic oxidation of ethyl lactate to ethyl pyruvate. The surface nitrogen dopant plays a vital role in this reaction, stabilizing the vanadium sites and tuning the catalyst electronic properties. Specifically, the active pyridinic N-oxide species formed in a high thermal-annealing treatment act synergistically with vanadium active sites, converting ethyl lactate with oxygen into ethyl pyruvate under mild conditions.

Acknowledgments

W. Zhang thanks the China Scholarship Council for a Ph.D. fellowship (201506140058). P. Oulego thanks the Spanish Ministry of Economy and Competitiveness (MINECO) (Project CTM2015-63864-R) and European Union (FEDER) for funding. This work is part of the Research Priority Area Sustainable Chemistry of the University of Amsterdam, http://suschem.uva.nl.

Conflict of Interest

The authors declare no conflict of interest.

Keywords: heterogeneous catalysis · biomass conversion · platform molecules · catalytic oxidation · synergistic effect · XPS

[1] M. Besson, P. Gallezot, C. Pinel, *Chem. Rev.* **2014**, *114*, 1827–1870.
[2] P. S. Shuttleworth, M. De bruyn, H. L. Parker, A. J. Hunt, V. L. Budarin, A. S. Matharu, J. H. Clark, *Green Chem.* **2014**, *16*, 573–584.
[3] R. Beerthuis, G. Rothenberg, N. R. Shiju, *Green Chem.* **2015**, *17*, 1341–1361.
[4] M. Dusselier, P. Van Wouwe, A. Dewaele, E. Makshina, B. F. Sels, *Energy Environ. Sci.* **2013**, *6*, 1415–1442.
[5] A. Corma, S. Iborra, A. Velty, *Chem. Rev.* **2007**, *107*, 2411–2502.
[6] P. Xu, J. Qiu, C. Gao, C. Ma, *J. Biosci. Bioeng.* **2008**, *105*, 169–175.
[7] S. Sugiyama, T. Kikumoto, H. Tanaka, K. Nakagawa, K.-I. Sotowa, K. Maehara, Y. Himeno, W. Ninomiya, *Catal. Lett.* **2009**, *131*, 129–134.
[8] N. Maleki, M. A. Eiteman, *Fermentatio* **2017**, *3*, 8.
[9] N. Maleki, M. Safari, M. A. Eiteman, *Eng. Life Sci.* **2018**, *18*, 40–47.
[10] S. Y. Lee, H. U. Kim, T. U. Chae, J. S. Cho, J. W. Kim, J. H. Shin, D. I. Kim, Y.-S. Ko, W. D. Jang, Y.-S. Jang, *Nature Catal.* **2019**, *2*, 18–33.
[11] E. Erlenmeyer, *Ber. Dtsch. Chem. Ges.* **1881**, *14*, 320–323.
[12] F. Howard, *Org. Syn. Coll.* **1941**, *1*, 475–476.
[13] S. C. A. Sousa, A. C. Fernandes, *Coord. Chem. Rev.* **2015**, *284*, 67–92.
[14] T. Mallat, A. Baiker, *Chem. Rev.* **2004**, *104*, 3037–3058.
[15] T. Tsujino, S. Ohigashi, S. Sugiyama, K. Kawashiro, H. Hayashi, *J. Mol. Catal.* **1992**, *71*, 25–35.
[16] H. Hayashi, S. Sugiyama, N. Shigemoto, K. Miyaura, S. Tsujino, K. Kawashiro, S. Uemura, *Catal. Lett.* **1993**, *19*, 369–373.
[17] S. Sugiyama, N. Shigemoto, N. Masaoka, S. Suetoh, H. Kawami, K. Miyaura, H. Hayashi, *Bull. Chem. Soc. Jpn.* **1993**, *66*, 1542–1547.
[18] S. Lomate, T. Bonnotte, S. Paul, F. Dumeignil, B. Katryniok, *J. Mol. Catal. A* **2013**, *377*, 123–128.
[19] H. Hayashi, S. Sugiyama, N. Masaoka, N. Shigemoto, *Ind. Eng. Chem. Res.* **1995**, *34*, 135–139.
[20] H. Hayashi, S. Sugiyama, T. Moriga, N. Masaoka, A. Yamamoto, *Stud. Surf. Sci. Catal.*, **1997**, 108. 421–428.
[21] K. T. Liu, X. M. Huang, E. A. Pidko, E. J. M. Hensen, *Green Chem.* **2017**, *19*, 3014–3022.
[22] X. Zhao, C. Zhang, C. Xu, H. Li, H. Huang, L. Song, X. Li, *Chem. Eng. J.* **2016**, *296*, 217–224.
[23] L. L. Zhang, R. K. Wang, L. Song, X. Y. Zhao, Q. M. Fan, H. Li, Q. Yu, X. B. Li, J. M. Zeng, C. H. Zhang, T. Liu, Z. W. Wang, *Catal. Lett.* **2019**, *149*, 840–850.
[24] T. Yasukawa, W. Ninomiya, K. Ooyachi, N. Aoki, K. Mae, *Ind. Eng. Chem. Res.* **2011**, *50*, 3858–3863.
[25] W. Zhang, G. Innocenti, P. Oulego, V. Gitis, H.-H. Wu, B. Ensing, F. Cavani, G. Rothenberg, N. R. Shiju, *ACS Catal.* **2018**, *8*, 2365–2374.
[26] W. Zhang, G. Innocenti, M. Ferbinteanu, E. V. Ramos Fernandez, A. Sepulveda-Escribano, H.-H. Wu, F. Cavani, G. Rothenberg, R. N. Shiju, *Catal. Sci. Technol.* **2018**, *8*, 3737–3747.
[27] E. V. Ramos-Fernandez, N. J. Geels, N. R. Shiju, G. Rothenberg, *Green Chem.* **2014**, *16*, 3358–3363.
[28] W. Zhang, B. Ensing, G. Rothenberg, R. N. Shiju, *Green Chem.* **2018**, *20*, 1866–1873.
[29] D. Eisenberg, W. Stroek, N. J. Geels, C. S. Sandu, A. Heller, N. Yan, G. Rothenberg, *Chem. Eur. J.* **2016**, *22*, 501–505.
[30] Y. Zhang, J. Diao, J. Rong, J. Zhang, J. Xie, F. Huang, Z. Jia, H. Liu, D. Su, *ChemSusChem* **2018**, *11*, 536–541.
[31] T. K. Slot, D. Eisenberg, D. van Noordenne, P. Jungbacker, G. Rothenberg, *Chem. Eur. J.* **2016**, *22*, 12307–12311.
[32] H. Yu, L. Shang, T. Bian, R. Shi, G. I. N. Waterhouse, Y. Zhao, C. Zhou, L.-Z. Wu, C.-H. Tung, T. Zhang, *Adv. Mater.* **2016**, *28*, 5080–5086.
[33] S. Kumar, N. Sharma, K. Kailasam, *J. Mater. Chem. A* **2018**, *6*, 21719–21728.
[34] T. K. Slot, D. Eisenberg, G. Rothenberg, *ChemCatChem* **2018**, *10*, 2119–2124.
[35] D. Zhao, Z. Xu, J. P. Chada, C. A. Carrero, D. C. Rosenfeld, J. L. Rogers, I. Hermans, G. W. Huber, *ACS Catal.* **2017**, 7479–7489.
[36] X. Wang, C.-G. Liu, D. Neff, P. F. Fulvio, R. T. Mayes, A. Zhamu, Q. Fang, G. Chen, H. M. Meyer, B. Z. Jang, S. Dai, *J. Mater. Chem. A* **2013**, *1*, 7920–7926.
[37] P. Yang, H. Ou, Y. Fang, X. Wang, *Angew. Chem. Int. Ed.* **2017**, *56*, 3992–3996; *Angew. Chem.* **2017**, *129*, 4050–4054.
[38] R. Arrigo, M. Hävecker, R. Schlögl, D. S. Su, *Chem. Commun.* **2008**, 4891–4893.
[39] G. P. Mane, S. N. Talapaneni, K. S. Lakhi, H. Ilbeygi, U. Ravon, K. Al-Bahily, T. Mori, D.-H. Park, A. Vinu, *Angew. Chem. Int. Ed.* **2017**, *56*, 8481–8485; *Angew. Chem.* **2017**, *129*, 8601–8605.
[40] Q. Gu, Y. Liao, L. Yin, J. Long, X. Wang, C. Xue, *Appl. Catal. B* **2015**, *165*, 503–510.
[41] T.-N. Tran, M. Y. Song, K. P. Singh, D.-S. Yang, J.-S. Yu, *J. Mater. Chem. A* **2016**, *4*, 8645–8657.

[42] J. Ma, N. Wu, S.-A. Sun, T. Yao, G.-Y. Li, T.-J. Hu, Y.-H. Li, X.-D. Li, *ChemCatChem* **2018**, *10*, 825–830.
[43] Z. Yang, Z. Liu, H. Zhang, B. Yu, Y. Zhao, H. Wang, G. Ji, Y. Chen, X. Liu, Z. Liu, *Chem. Commun.* **2017**, *53*, 929–932.
[44] D. Eisenberg, T. K. Slot, G. Rothenberg, *ACS Catal.* **2018**, 8618–8629.
[45] P. Zhang, Y. Gong, H. Li, Z. Chen, Y. Wang, *Nat. Commun.* **2013**, *4*, 1593.
[46] Q.-Y. Bi, J.-D. Lin, Y.-M. Liu, H.-Y. He, F.-Q. Huang, Y. Cao, *Angew. Chem. Int. Ed.* **2016**, *55*, 11849–11853; *Angew. Chem.* **2016**, *128*, 12028–12032.
[47] X. Cui, A.-E. Surkus, K. Junge, C. Topf, J. Radnik, C. Kreyenschulte, M. Beller, *Nat. Commun.* **2016**, *7*, 11326.
[48] M. Qiao, C. Tang, G. He, K. Qiu, R. Binions, I. P. Parkin, Q. Zhang, Z. Guo, M. M. Titirici, *J. Mater. Chem. A* **2016**, *4*, 12658–12666.
[49] N. Tawil, E. Sacher, E. Boulais, R. Mandeville, M. Meunier, *J. Phys. Chem. C* **2013**, *117*, 20656–20665.
[50] D. Yang, A. Velamakanni, G. Bozoklu, S. Park, M. Stoller, R. D. Piner, S. Stankovich, I. Jung, D. A. Field, C. A. Ventrice, R. S. Ruoff, *Carbon* **2009**, *47*, 145–152.
[51] Y. Wang, H. J. Zhang, A. S. Admar, J. Luo, C. C. Wong, A. Borgna, J. Lin, *RSC Adv.* **2012**, *2*, 5748–5753.
[52] Q. Tang, Y. Chen, Y. Yang, *J. Mol. Catal. A* **2010**, *315*, 43–50.

Manuscript received: May 4, 2019
Accepted manuscript online: May 30, 2019
Version of record online: July 1, 2019